Thermodynamic Role of Glutathione Oxidation by Peroxide and Peroxybicarbonate in the Prevention of Alzheimer's Disease and Cancer

Natalie J. Galant,[†] Hui Wang,[‡,§] DongJin R. Lee,[†] Zoltan Mucsi,[†] David H. Setiadi,[†,||] Bela Viskolcz,*[,§,⊥] and Imre G. Csizmadia[†,§,||,⊥,#]

Department of Chemistry, University of Toronto, Toronto, Ontario, Canada M5S 3H6, College of Chemistry, Beijing Normal University, Xin Wai Street 19, Hai Dian, Beijing, 100875, China, and Department of Chemical Informatics, Faculty of Education, University of Szeged, Boldogasszony sgt. 6, Szeged, Hungary 6725

Received: October 15, 2008; Revised Manuscript Received: May 26, 2009

First principle quantum molecular computations have been carried out at the B3LYP/6-31G(d,p) and G3MP2B3 levels of theory on ethyl mercaptan and diethyl disulfide to study their full conformational space. The consequences of molecular axis chirality for the potential energy hypersurface of diethyl disulfide was fully explored. Thermodynamic functions (U, H, S, and G) have been computed for every conformer of the products as well as the reactants of the redox systems studied. Relative values of the thermodynamic functions were calculated with respect to the reference structures with anti orientation. The energetics of the following Red-Ox reactions

$$Et{-}SH + HO{-}OH + HS{-}Et \rightarrow 2H_2O + Et{-}S{-}S{-}Et$$

$$Et{-}SH + HO{-}OCOO^{(-)} + HS{-}Et \rightarrow H_2O + Et{-}S{-}S{-}Et + HCO_3^-$$

have been chosen to mimic the biologically important Red-Ox reactions of glutathione

$$G{-}SH + H_2O_2 + HS{-}G \rightarrow 2H_2O + G{-}S{-}S{-}G$$

$$G{-}SH + HCO_4^- + HS{-}G \rightarrow H_2O + G{-}S{-}S{-}G + HCO_3^-$$

The Red−Ox reaction of Et−SH → Et−S−S−Et was found to be exothermic by first principle molecular computations and the intramolecular interactions, such as the unusual C−H···H−C noncovalent bondings were studied by Bader's atoms in molecules analysis of the electron density topology. The present paper focuses attention on the thermodynamic aspect of the redox reaction of glutathione. It has been noted previously that on going from a cancerous to a healthy cell, the entropy change is negative, corresponding to information accumulation. Likewise, the dissociation of peptide parallel β-sheets, that dominate the plaques in Alzheimer's Disease, governs negative entropy change. It may be interesting to note, according to the results obtained in the present paper, a negative entropy change, corresponding to information accumulation.

1. Introduction

1.1. Background to Oxidative Stress. It has been known for several decades that oxidative stress is dangerous to most aerobic organisms. As Harmon dramatically pointed out for the first time, in 1954, in connection with the free radical and aging: "Very few individuals, if any, reach their potential maximum lifespan; they die instead prematurely of a wide variety of diseases - the vast majority being 'free radical' diseases".[1] This is due to the fact that the oxidation in the cell requires oxygen, and this wet-combustion occurs in the mitochondria. This mitochondrial process produces ATP (oxidative phosphorylation) in which H_2O is produced from O_2 by biochemical reduction. However, 1 in every 20 molecules of O_2 is retained by the body, as it escapes the full reduction process to H_2O (Figure 1).

The role of oxidative stress in virulent diseases, atherosclerosis, diabetes, chronic inflammation, and ischemia, is widely recognized.[2−7] Increased expression of proto-oncogenes, as well as damage to proteins, DNA, and tumor suppressor genes, may be the result of ROS and oxidative damage.[8−10]

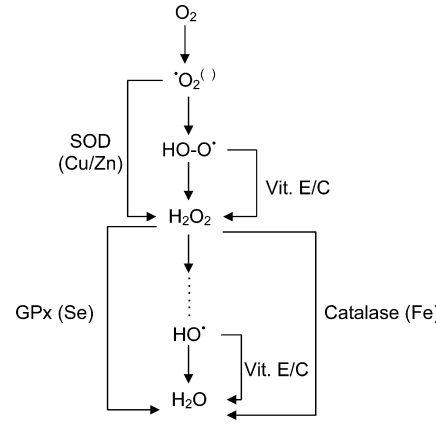

Figure 1. Schematic representation of the nonenzymatic (antioxidant) and enzymatic mitochondrial reduction process of O_2 to H_2O. Such a process produces reactive oxygen species (ROS), as reaction intermediates, such as hydrogen peroxide (H_2O_2) and free radicals such as $^{\bullet}O_2^-$, $HO^{\bullet}$, and $HO{-}O^{\bullet}$.

It is currently believed that over sixty degenerative diseases are the result of oxidative stress.[11] Among these are the most highly prevalent diseases: Alzheimer's Disease, cancer, and type

* To whom correspondence should be addressed.
[†] University of Toronto.
[‡] Beijing Normal University.
[§] University of Szeged.
[||] Global Institute of Molecular and Materials Science (www.giocomms.org).
[⊥] Drug Discovery Research Center (www.drugcent.com).
[#] International Scientific Consultants Inc.

10.1021/jp809116n CCC: $40.75
Published on Web 07/22/2009

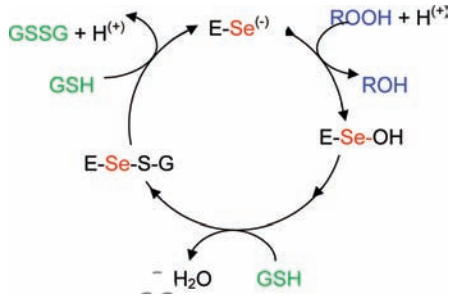

Figure 2. Catalytic cycle of GPx demonstrating the oxidative mechanism of GSH to GSSG.

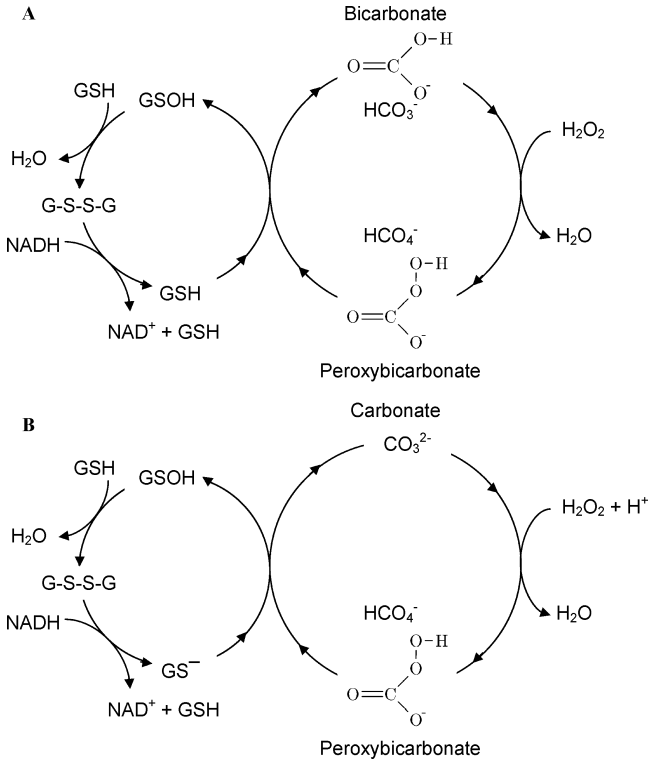

Figure 3. Putative mechanism of the catalytic effect of two peroxybicarbonate cycles for the oxidation of glutathione: $2GSH + H_2O_2 \rightarrow GSSG + 2H_2O$. (A) The oxidation starts with GSH. (B) The oxidation starts with GS(-) following the work of Regino and Richardson.[14]

2 diabetes.[1,12] Antioxidants, such as vitamins C and E, assist in the prevention of tissue damage by trapping free radicals such as HO−O• and HO•, whereas other ROS intermediates may be removed through other enzymatic processes (Figure 1). The one case of enzymatic ROS removal includes glutathione peroxidase (GPx), which leads to H_2O_2 removal. The GPx enzyme's selenium atom of the selenocysteine residue, located at the enzymatic active site, temporarily picks up an OH from H_2O_2 and uses this oxygen subsequently to oxidize GSH (Figure 2).[13]

On the basis of a systematic study[14] involving cysteine and related thiols, one may construct an alternative mechanism for the oxidation of glutathione (GSH). In such a putative mechanism (Figure 3), bicarbonate ion (HCO_3^-) may act as an oxygen carrier. In this case, instead of selenocysteine (Figure 2), the catalytic effect of bicarbonate involves the formation of peroxybicarbonate (HCO_4^-), which may then carry out oxidation of the thiol as illustrated in Figure 3.

1.2. Oxidative Stress and Alzheimer's Disease. Numerous soluble proteins (lysosime, myoglobulin, etc.) tend to aggregate,[15,16] virtually irreversibly, to insoluble structures that may be viewed as a "dead-end street of protein folding".[17] The amyloid plaques

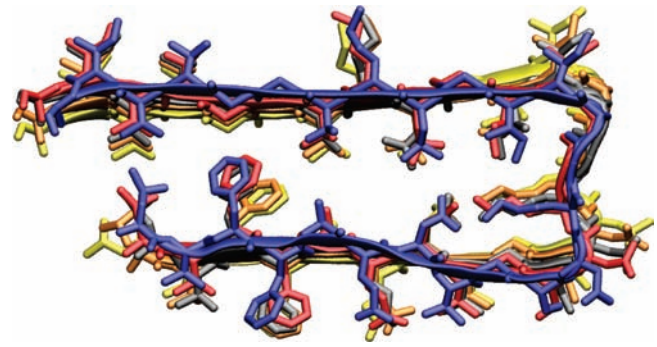

Figure 4. Structure of an amyloid peptide aggregate model.

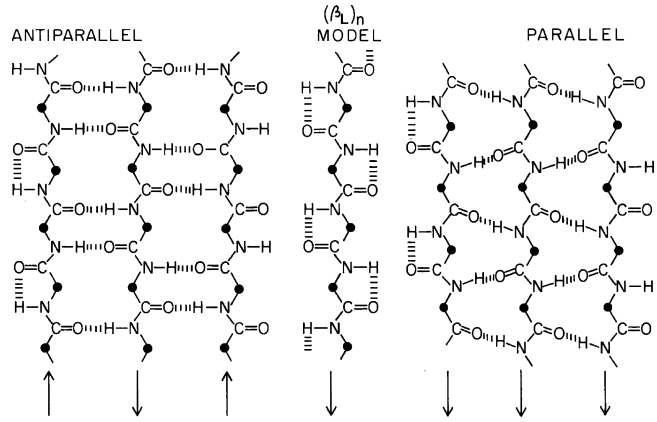

Figure 5. Parallel β-strand (at the right) has relatively weak hydrogen bonds, and each of the single strands (shown at the center) can be broken-off one at the time.

occurring in Alzheimer's disease are the most widely recognized structural features.[18,19] Figure 4 clearly illustrates the structural features of such plaques.[20]

The plaques consist of parallel β-sheets folded back at about the middle of the chains. Even though parallel β-sheet interactions are weaker than antiparallel β-sheets (Figure 5), the aggregate is very stable and resists dispersion of individual polypeptide chains due to the many hydrogen bonds involved.

It is still an open question what abnormal cellular conditions lead to protein misfolding that result in these pathogenic aggregations. The full understanding of the amyloid type aggregate formation mechanism some day may lead to prevention.[21]

One of the first events that occur in the initiation of Alzheimer's disease is oxidative stress.[22] Cells normally have low ROS levels due to NADPH oxidase, and concentrations of ROS, such as H_2O_2, may be regulated by glutathione. The brain has a greater risk being susceptible to ROS damage, and thus initiation of neurodegenerative diseases such as Parkinson's and Alzheimer's disease, due to its high rate of metabolism and decreased cell regeneration ability. Evidence of this exists as reports of protein oxidation have been found in the hippocampus and neocortex of Alzheimer's patients.[23]

Some researchers assume that free radicals pull-off an H-atom from amino acid α-carbons located in the polypeptide chains which will make the α carbon planar and that could trigger the planar amyloid structure formation.[24,25] For this reason, the GSH content of the brain cell is very important to prevent the initiation of Alzheimer's Disease. Since GSH is an intracellular antioxidant, it cannot pass through the blood−brain barrier; therefore, only the component amino acids can be supplied externally as one possible preventive measure.[26] The inability of GSH to pass

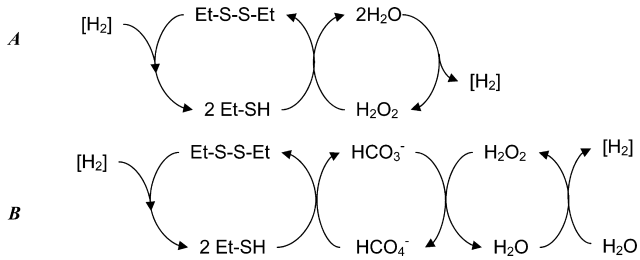

Figure 6. Red-Ox reaction models involving Et−SH and Et−S−S−Et. (A) Direct oxidation of Et−SH to Et−S−S−Et by H_2O_2. (B) Bicarbonate catalyzed oxidation of Et−SH to Et−S−S−Et by H_2O_2. Direct hydrogenation reaction are illustrated in both A and B.

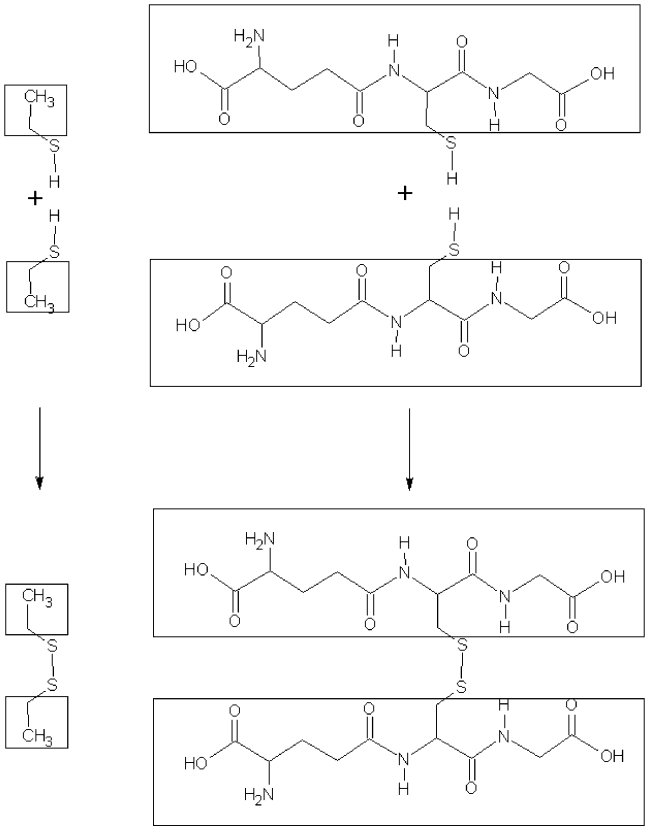

Figure 7. Emphasis of chemical changes from SH to SS functionalities through oxidation of glutathione oxidation and its model, ethyl mercaptan.

easily through the blood−brain barrier[26] confirms that GSH is an important intracellular antioxidant that must be well understood before any action toward successfully preventing such diseases is taken.

Any changes in glutathione homeostasis is believed to be the result of oxidative stress and be responsible for neurological diseases, such as Alzheimer's and Parkinson's disease, as depletion of GSH may result in apoptosis.[26] Throughout an organism's lifetime, GSH levels deplete, thus allowing for an increase in oxidative stress and the amount of accumulative damage it may cause to tissues.

1.3. Oxidative Stress and Cancer. Some suggest that cancer may be a genetic disease due to the accumulation of genetic mutations in cell proliferation, genomic instability, and cell death genes.[27] For many years, such a theory, commonly referred to as the somatic mutation theory of cancer, has been the major explanation for the carcinogenic process. It is only now that alternate theories are being considered as the previously mentioned hypothesis may not explain new carcinogenic

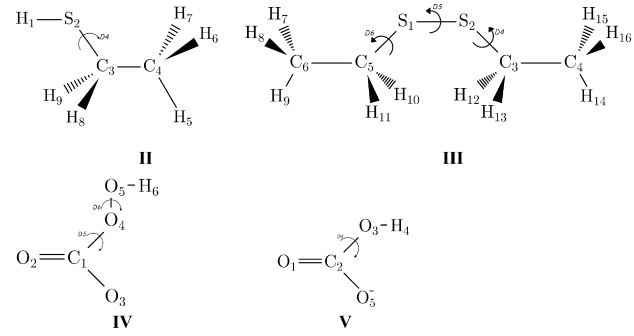

Figure 8. Atomic numbering system for Et−SH (**II**), Et−S−S−Et (**III**), peroxybicarbonate (**IV**), and bicarbonate (**V**). The definitions of the dihedral angles used in II were $H_1S_2-C_3C_4$ (D4) and for **III**, $S_1S_2-C_3C_4$ (D4), $C_3S_2-S_1C_5$ (D5), $S_2S_1-C_5C_6$ (D6) were used. For **IV**, dihedrals were defined as $O_5O_4-C_1O_2$ (D5), $H_6O_5-O_4C_1$ (D6), and for **V** as $H_4O_1-C_2O_3$ (D4).

research findings.[28−31] Increased ROS production has been found to originate from muscle mitochondria, commonly referred to as mitochondrial oxidative stress. Research now suggests that cellular H_2O_2 concentration increases are the hallmarks of cancer.[32,33] H_2O_2 increase is also associated with genetic instability.[34−39] The highly reactive OH radical is generated from H_2O_2 via the Fenton mechanism.[34,38,39] Research has found that cell proliferation,[16,40,41] apoptosis resistance,[42,43] increased angiogenesis,[44,45] invasion, and metastasis[41,46,47] may be induced by H_2O_2. However, studies suggest that H_2O_2-detoxifying enzyme increases could result in apoptosis promotion, cell proliferation reduction, and metastasis, invasion, and angiogenesis inhibition. Pathological changes, which are indicative for dysregulation of signal cascades or gene expression, are often coupled with changes in intracellular glutathione levels.[48] Studies has also found that H_2O_2 can result in malignant transformation induction[49−52] and phenotypic reversal of H_2O_2-detoxifying enzymes, such as glutathione peroxidase or catalase in cancer cells.[51,53,54] In general, an increased H_2O_2 production in cancer cells, as well as increased ROS levels within a cell, have been found to be related to the hallmarks of cancer.

1.4. Molecular Structure. Glutathione (GSH, I), a tripeptide, has an unusual amino acid sequence (L-γ-glutamyl-L-cysteinylglycine) due to peptide bond formation involving a glutamic acid and using its side chain, i.e., its COOH moiety located at the γ-carbon rather than the usual α-carbon carboxylic acid,[55] is also one of the most abundant (0.1−10 mM) intracellular nonprotein thiols.[56]

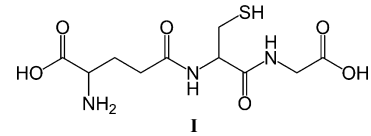

I

Initially isolated in 1929,[57] its full synthesis came several decades later,[58] whereas its metabolism was established in 1983.[59] GSH's critical antioxidant abilities lie in its thiol (−SH) functional group,[56] which may be oxidized to a disulfide (−S−S−) linkage according to (1)

$$G-SH + H_2O_2 + HS-G \rightarrow 2H_2O + G-S-S-G \quad (1)$$

1.5. Biological Synthesis. Synthesized intracellularly by two consecutive reactions[60] through the initial production of L-

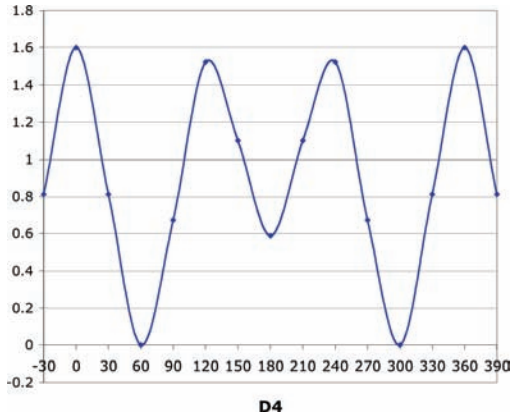

Figure 9. Potential energy curve (PEC) of ethyl mercaptan. The dependent variable is relative energy (kCal mol^{-1}) whereas the independent variable is D4 = $H_1S_2-C_3C_4$. Points plotted were optimized at B3LYP/6-31G(d,p).

glutamyl-L-cysteine dipeptide catalyzed by γ-glutamylcysteinyl synthetase:

$$\text{L-Glutamic acid} + \text{L-cysteine} + \text{ATP} \rightarrow \text{L-glutamyl-L-cysteine} \quad (2)$$

The second step involves the catalysis of GSH formation by GSH synthetase:

$$\text{L-Glutamyl-L-cysteine} + \text{glycine} + \text{ATP} \rightarrow \text{GSH} \quad (3)$$

1.6. Peroxybicarbonate and Bicarbonate. When one of the largest components of extracellular fluid buffers, bicarbonate (HCO_3^-), is present in concentrations greater than 25 mM, thiol oxidation is increased by a factor ≥ 2.[14] The present study focuses on the role bicarbonate plays as in GSH oxidation it temporarily arrests H_2O_2 and is converted to peroxybicarbonte.[61] Peroxybicarbonate acts as an additional oxidization agent, which will be further studied in this GSH oxidation reaction model.

1.7. Scope of Research. ***1.7.1. Neutral Thermodynamics.*** This current study aims to mimic the initial and final states of the GSH to GSSG Red−Ox reaction via modeling the large GSH molecule by ethyl mercaptan (Et−SH). Such a systematic model (Figure 6) shall be used in hopes of revealing of the intricacies of the nonenzymatic directed Red-Ox reaction of GSH to GSSG as specified by (4a)

$$\text{Et}-\text{SH} + H_2O_2 + \text{HS}-\text{Et} \rightarrow 2H_2O + \text{Et}-\text{S}-\text{S}-\text{Et} \quad (4a)$$

$$HCO_3^- + H_2O_2 \rightarrow HCO_4^- + H_2O \quad (4b)$$

$$2\text{Et}-\text{SH} + HCO_4^- \rightarrow \text{Et}-\text{S}-\text{S}-\text{Et} + H_2O + HCO_3^- \quad (4c)$$

The equilibrium constant for reaction 4b has an appreciably high value, $K_{eq} = 0.33$.[60]

Direct oxidation reactions 4a are shown in Figure 6A and catalytic oxidation reactions according to 4b and 4c are illustrated in Figure 6B.

All reactions studied are in the gas phase. The gas phase reaction is regarded as primary reference. All future environmental study of various dielectric constant (in aqueous solutions or in membranes) will be compared to the present study.

1.7.2. Anionic Thermodynamics. An additional reaction was studied which uses the deprotenated form of Et-SH as a reactant to study the thermodynamics of the reaction when an anionic reactant is used. The proposed reaction is depicted as follows 5a:

$$\text{Et}-S^- + HCO_4^- \rightarrow \text{Et}-\text{SOH} + CO_3^{2-} \quad (5a)$$

$$\text{Et}-\text{SOH} + \text{HSEt} \rightarrow \text{Et}-\text{S}-\text{S}-\text{Et} + H_2O \quad (5b)$$

This mechanism, proposed by Regino and Richardson,[14] is already depicted in Figure 3B. Utilization of simple models may allow for the mimicking of the bioactive molecules, GSH and GS−SG, as it is the thiol group (−SH) that suffers the greatest amount of chemical change during the oxidation process. The other groups attached to the SH moiety of lesser importance, as illustrated in Figure 7.

2. Methods

2.1. Molecular Structure and Stability. All calculations were carried out using the Gaussian 03 (G03) program.[62] Three levels of theory were used on each respective molecular structure. Molecular structures were first optimized using RHF/3-21G, which yielded geometrical optimized structural parameters that were then used as an input in a subsequent theoretical refinement which allowed the inclusion of electron correlation effects at B3LYP/6-31G(d,p), denoted as method A, thus obtaining more reliable geometry and stability data.[63] The preceding levels of theory included multi-dimensional conformational analysis (MDCA).[64] Total energies and the thermodynamic functions (U, H, and G) are given in hartrees, and their relative values were calculated in kilocalories per mole using the following conversion factor: 1 hartree = 627.5095 kcal mol^{-1}. The entropy and its relative values are given in cal(mol K)$^{-1}$. Subsequently, molecular structures were subjected to even a higher level of theory to yield more accurate energies at all stationary points using G3MP2B3, denoted as

TABLE 1: Optimized Energy Values Computed at B3LYP/6-31G(d,p) and G3MP2B3 Levels of Theory for Conformational Change Involving Rotation about the C−S Bond (D4) in Ethyl Mercaptan Using the Conversion Factor of 1 hartree = 627.5095 kcal mol^{-1}

D4	*U* (Hartree)	*H* (Hartree)	*G* (Hartree)	*S* (cal(mol K)$^{-1}$)	Δ*U* (kcal/mol)	Δ*H* (kcal/mol)	Δ*G* (kcal/mol)	Δ*S* (cal(mol K)$^{-1}$)
				Method A: B3LYP/6-31G (d,p)				
±60	−477.944044	−477.943100	−477.975314	67.8	−0.6	−0.6	−0.4	−0.7
180	−477.943095	−477.942151	−477.974706	68.5	0.0	0.0	0.0	0.0
				Method B: G3MP2B3				
±60	−477.408249	−477.407304	−477.439672	67.8	−0.5	−0.5	−0.3	−0.7
180	−477.407452	−477.406508	−477.439191	68.4	0.0	0.0	0.0	0.0

TABLE 2: AIM Determined Parameters of Et−SH

bond/angle/cage vertical point	anti		gauche (−)		gauche (+)	
	r_b	ρ_b	r_b	ρ_b	r_b	ρ_b
S−H	1.35104	0.202267	1.35166	0.202057	1.35166	0.202055

method B, allowing for the calculation of more reliable frequency and thermodynamic functions.

The atoms in the molecular structures of Et−SH (**II**), its oxidized form Et−S−S−Et (**III**) as well as peroxybicarbonate (**IV**) and bicarbonate ion (**V**) were each numbered in the following fashion (Figure 8):

2.2. Potential Energy Curves and Surfaces. The dihedral angles for **II** were taken as $H_1S_2-C_3C_4$ (D4), and for **III** as $S_1S_2-C_3C_4$ (D4), $C_3S_2-S_1C_5$ (D5), $S_2S_1-C_5C_6$ (D6) were taken in these preliminary truncated models which are sampled at gauche$^+$ (g^+), anti (a), and gauche$^-$ (g^-), to search for all probable conformers at gas phase, 0 K. The dihedral angles for peroxybicarbonate (**IV**) were taken as $O_5O_4-C_1O_2$ (D5), $H_6O_5-O_4C_1$ (D6) and as $H_4O_3-C_2O_1$ (D4) for bicarbonate (**V**) and In the case of Et-SH, the potential energy curve (PEC) of the form 6 was investigated:

$$\Delta E = f[\mathrm{D4}] \tag{6}$$

The potential energy hypersurface (PEHS) of Et−S−S−Et can be described by 7:

$$\Delta E = f[\mathrm{D4}, \mathrm{D5}, \mathrm{D6}] \tag{7}$$

two-dimensional constructions, i.e., potential energy surfaces (PES), of 1 were investigated with dihedral angle D5 set and optimized at either +90° or −90°.

$$\Delta E_{\mathrm{D5}} = f[\mathrm{D4}, \mathrm{D6}] \tag{8}$$

2.3. Topological Analysis of Electron Density (AIM Analysis). Electron density calculations were also completed to investigate whether there existed a possibility of intermolecular interactions. From optimized structures, intramolecular interactions, such as S···H−C and C−H···H−C, were identified on the basis of bond distances between the atoms covalently not bonded. Interatomic distances were differentiated based criteria that shorter bond lengths (Å) were characteristic of a higher interaction strength.[62,65,66] These interactions were also subjected to Baders atoms in molecules (AIM) analysis.[67,68]

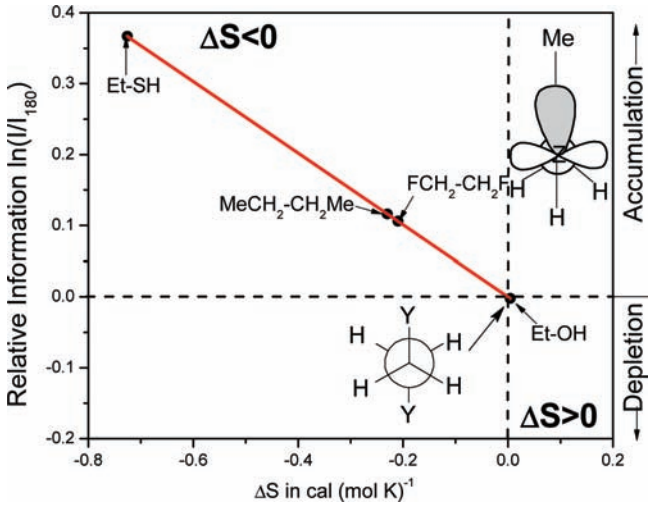

Figure 10. Logarithmic relative information content values of gauche conformers with respect to the anti orientation of previously studies compounds (Et−OH, FCH_2-CH_2F, $MeCH_2-CH_2Me$) and ethyl mercaptan (Et−SH). Note: Z = S or O and Y = F or Me.

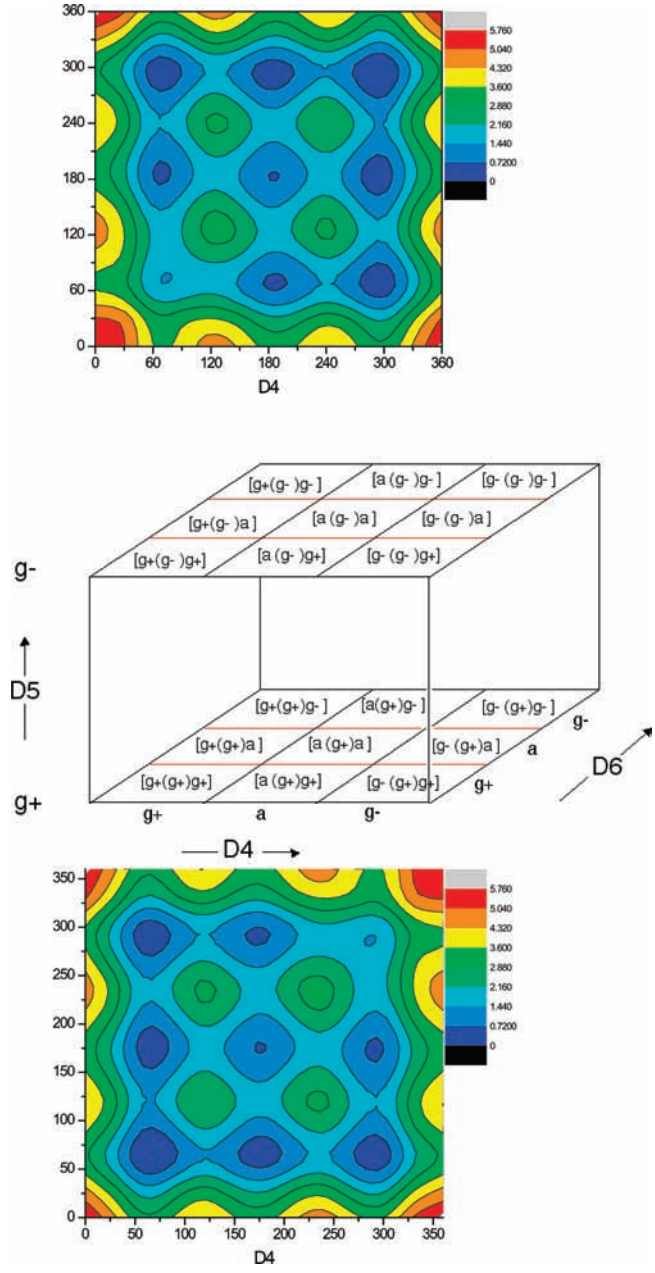

Figure 11. Potential energy surface cross sections (PES) of the potential energy hypersurface (PEHS) according to 7. Each floor corresponds to a different rotation about the disulfide bond. The conformers of opposite position, such as [g^+, g^+, g^+] and [g^-, g^-, g^-], are in enantiomeric relationship and therefore have identical energies. The chirality of the two cross sections (g^+ on the bottom and g^- on the top) are clearly seen.

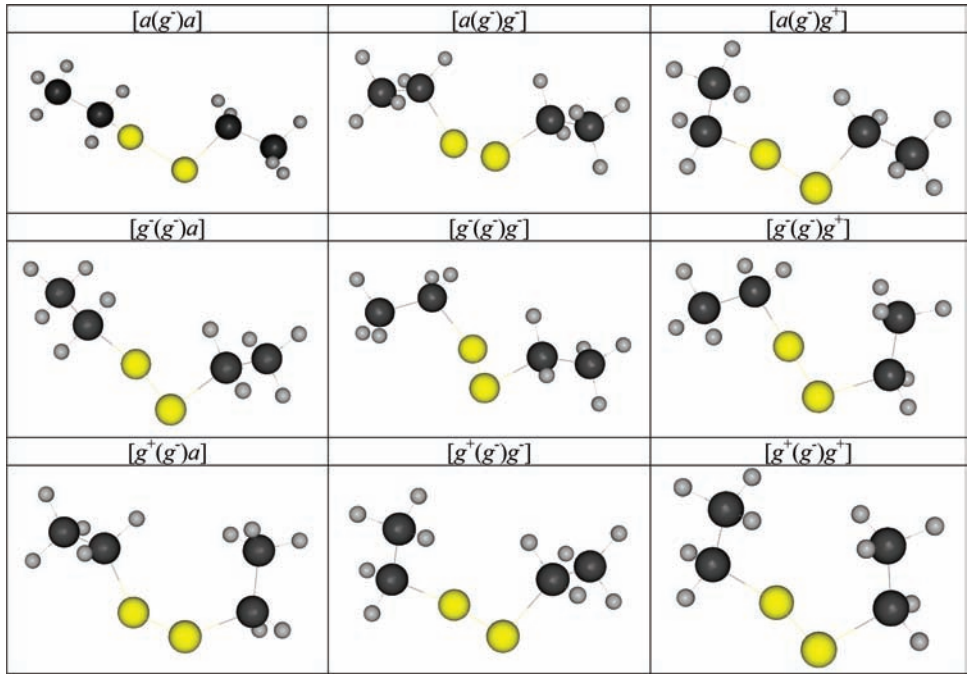

Figure 12. Stereospecific representation of the D4 = g^- conformers of diethyl disulfide optimized at B3LYP/6-31G(d,p) level of theory.

2.4. Information Accumulation via Entropy Change. By measuring the thermodynamic state function change for a conformation change or chemical reaction, the degree of stabilization may be obtained. The change in degree of disorder (ΔS) and reaction driving force (ΔG) both comprise the enthalpy change (ΔH) of a reaction:

$$\Delta H = \Delta G + T\Delta S \tag{9}$$

where a relationship exists between the ΔG and the equilibrium constant of the reaction

$$\Delta G = -RT \ln K_{\text{reaction}} \tag{10}$$

where K_{reaction} is a dimensionless quantity for bimolecular processes yielding two product molecules.

The change in disorder (ΔS) or a change of order ($-\Delta S$) provides a method of quantifying the relative structural information (I/I_0) associated with the reaction:[69−73]

$$\left(\frac{I}{I_0}\right) = e^{-(1/R)\Delta S} \quad \text{or} \quad \ln\left(\frac{I}{I_0}\right) = -\left(\frac{1}{R}\right)\Delta S \tag{11}$$

Because of this, ΔS measures the structural information change and with the flow of enthalpy (ΔH) the entropy (ΔS) also flows. The flow of entropy in one direction is equivalent therefore with the flow of information in the opposite direction according to 10. Thus the entropy or information flow may be important in mercaptan oxidation as well as disulfide reduction.

In view of the foregoing, the equilibrium constant (K_{reaction}) may also be written in the following ways:

$$K_{\text{reaction}} = \mathrm{e}^{-(1/RT)\Delta G} = \mathrm{e}^{+(1/R)\Delta S}\mathrm{e}^{-(1/RT)\Delta H} = [I_0/I]\mathrm{e}^{-(1/RT)\Delta H} \tag{12}$$

3. Results and Discussion

3.1. Ethyl Mercaptan (Et−SH). ***3.1.1. Conformation Analysis of Ethyl Mercaptan.*** In ethyl mercaptan (Et−SH), the terminal methyl group always occupies the same spatial orientation therefore rotation about only the C−S bond represents an important independent variable for conformational change as indicated in 6. The variation of energy with dihedral angle D4 associated with the rotation about the C−S bond is shown in Figure 9. The actual total energies associated with the optimized minima are summarized in Table 1. The optimized molecular parameters are tabulated in the Supporting Information (Table S1).

As can be seen from Table 1 and Figure 9, the gauche conformation is more stable than the anti in contrast to the general understanding of molecular conformation that anti arrangements are usually the global minima. There are known examples in the literature whereby the gauche structure is more stable than anti, this is usually referred to as the gauche-effect. It happens in the case of carbohydrates where two oxygen atoms (or two different heteroatoms) are connected to the anomeric carbon (C_1) of hexoses. In such cases, the phenomenon is usually referred to as the anomeric-effect. It also happens occasionally for larger heteroatoms such as sulfur.[74,75]

The frequency and intensity values are listed in Table S2a of the Supporting Information, as well as the vibrational spectra for the gauche and anti conformers (Figure S1).

3.1.2. AIM Analysis of Electron Density Topology of Et-SH. The molecular structures containing the pertinent details of the AIM analysis of ET−SH are shown in Figure S4. Table 2 summarizes the most important parameters (r_b and ρ_b) determined by AIM analysis for Et-SH in its anti and gauche conformers.

3.1.3. Structural Informational Content of Et−SH. On going from anti to gauche conformation, rotation about a C−O bond in Et−OH leads to a very small information depletion.[75] In contrast to that, rotation about the C−C bond, in $MeCH_2-CH_2Me$ and FCH_2-CH_2F, exhibits a modest information accumulation.[72,73] However, in the case of Et-SH, rotation

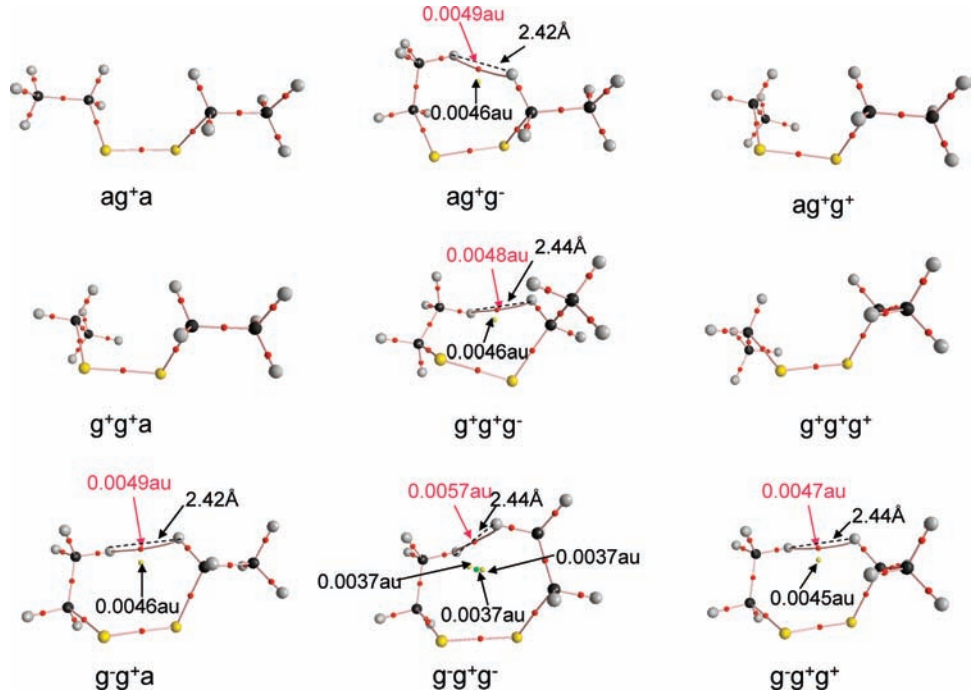

Figure 13. AIM analysis results of Et−S−S−Et performed at the level of B3LYP/6-31G(d). Interaction distances are given in Å and bond critical point electron density (ρ_b) is shown in atomic units (au).

TABLE 3: Structural and Thermodynamic Characteristics of H_2 Computed at Two Levels of Theory

R	*E* (Hartree)	*U* (Hartree)	*H* (Hartree)	*G* (Hartree)	*S* (cal/(mol K)$^{-1}$)
		Method A: B3LYP/6-31G(d,p)			
0.743 Å	−1.17853933613	−1.166005	−1.165061	−1.179853	31.132
		Method B: G3MP2B3			
0.743 Å	−1.180383	−1.168283	−1.167339	−1.182131	31.132

TABLE 4: Disulfide Linkages (Å) of Et−S−S−Et for Various Conformers Optimized at B3LYP/6-31G(d,p) (Method A) and G3MP2B3 (Method B) Levels of Theory Rotating about D4 and D6 when D5 = $g^{\pm}$, As Well As Enthalpy ΔH_{Hydrog} (kcal mol^{-1}), Free Energy ΔG_{Hydrog} (kcal mol^{-1}), and Entropy ΔS (cal(mol K)$^{-1}$) Thermodynamic Functions of H_2

			method A: B3LYP/6-31G (d,p)				method B: G3MP2B3		
code	[D4(D5)D6]	S−S	ΔH_{Hydrog}	ΔG_{Hydrog}	ΔS_{Hydrog}	code	ΔH_{Hydrog}	ΔG_{Hydrog}	ΔS_{Hydrog}
1(g^+)-A	[g^+(g^+)g^+]	2.0838	−8.6	−12.0	11.3	**1**(g^+)-B	−3.5	−6.8	11.2
2(g^+)-A	[g^-(g^+)g^+]	2.0857	−9.0	−12.4	11.5	**2**(g^+)-B	−3.7	−7.0	11.4
3(g^+)-A	[a(g^+)g^+]	2.0822	−9.1	−11.9	9.3	**3**(g^+)-B	−4.1	−6.8	9.3
4(g^+)-A	[g^+(g^+)a]	2.0822	−9.1	−11.9	9.3	**4**(g^+)-B	−4.1	−6.8	9.3
5(g^+)-A	[g^-(g^+)a]	2.0834	−9.4	−12.4	10.2	**5**(g^+)-B	−4.3	−7.3	10.1
6(g^+)-A	[a(g^+)a]	2.0795	−9.5	−12.3	9.1	**6**(g^+)-B	−4.9	−7.5	9.1
7(g^+)-A	[g^+(g^+)g^-]	2.0857	−9.0	−12.4	11.5	**7**(g^+)-B	−3.7	−7.0	11.4
8(g^+)-A	[a(g^+)g^-]	2.0834	−9.4	−12.5	10.2	**8**(g^+)-B	−4.3	−7.3	10.1
9(g^+)-A	[g^-(g^+)g^-]	2.0913	−10.1	−13.3	10.6	**9**(g^+)-B	−5.1	−8.1	10.5
1(g^-)-A	[g^+(g^-)g^+]	2.0913	−10.1	−13.3	10.6	**1**(g^-)-B	−5.1	−8.1	10.5
2(g^-)-A	[a(g^-)g^+]	2.0834	−9.4	−12.5	10.2	**2**(g^-)-B	−4.3	−7.3	10.1
3(g^-)-A	[g^-(g^-)g^+]	2.0857	−9.0	−12.4	11.5	**3**(g^-)-B	−3.7	−7.0	11.4
4(g^-)-A	[a(g^-)a]	2.0795	−9.5	−12.3	9.1	**4**(g^-)-B	−4.9	−7.5	9.1
5(g^-)-A	[g^+(g^-)a]	2.0835	−9.4	−12.4	10.2	**5**(g^-)-B	−4.3	−7.3	10.1
6(g^-)-A	[g^-(g^-)a]	2.0822	−9.1	−11.9	9.3	**6**(g^-)-B	−4.1	−6.8	9.3
7(g^-)-A	[a(g^-)g^-]	2.0822	−9.1	−11.9	9.3	**7**(g^-)-B	−4.1	−6.8	9.3
8(g^-)-A	[g^+(g^-)g^-]	2.0858	−9.0	−12.4	11.4	**8**(g^-)-B	−3.7	−7.0	11.4
9(g^-)-A	[g^-(g^-)g^-]	2.0839	−8.6	−12.0	11.3	**9**(g^-)-B	−3.5	−6.8	11.2

about the C−S bond shows a noticeably larger effect [$\ln(I/I_0) = +0.367$ and $(I/I_0) = 1.443$] as illustrated graphically in Figure 10.

3.2. Diethyl Disulfide (Et−S−S−Et). ***3.2.1. Conformational Analysis of Diethyl Disulfide.*** In diethyl disulfide (Et−S−S−Et), the terminal methyl groups always occupy the same spatial orientation. Therefore, only three dihedral angles (D4, D5, and D6) are important independent variables for conformational changes according to 7. The topological arrangement of the potential energy hypersurface, represented by 7, is shown in Figure 11. These are comparable to those published by Haworth.[76] Our surface is virtually identical to the CS−SC dihedral angle 90° cross-section of their 3D hypersurface of the Haworth paper.[76] These are the true minima[76] that we have used to study the red-ox reaction of diethyldisulfide.

TABLE 5: Relative Information Content Values (I/I_0) and Their Logarithmic Equivalent of the Various Conformers of Diethyl Disulfide (Et−S−S−Et)

code	[D4(D5)D6]	ΔS (cal(mol K)$^{-1}$)	$-\Delta S/R = \ln(I/I_0)$	(I/I_0)
		Method A: B3LYP/6-31G (d,p)		
1(g^+)-A	[$g^+(g^+)g^+$]	−2.2	1.103	3.014
2(g^+)-A	[$g^-(g^+)g^+$]	−2.4	1.185	3.272
3(g^+)-A	[$a(g^+)g^+$]	−0.2	0.120	1.127
4(g^+)-A	[$g^+(g^+)a$]	−0.2	0.117	1.124
5(g^+)-A	[$g^-(g^+)a$]	−1.1	0.534	1.706
6(g^+)-A	[$a(g^+)a$]	0.0	0.000	1.000
7(g^+)-A	[$g^+(g^+)g^-$]	−2.4	1.189	3.285
8(g^+)-A	[$a(g^+)g^-$]	−1.1	0.556	1.744
9(g^+)-A	[$g^-(g^+)g^-$]	−1.5	0.752	2.121
		Method B: G3MP2B3		
1(g^+)-B	[$g^+(g^+)g^+$]	−2.1	1.076	2.932
2(g^+)-B	[$g^-(g^+)g^+$]	−2.3	1.152	3.165
3(g^+)-B	[$a(g^+)g^+$]	−0.2	0.105	1.111
4(g^+)-B	[$g^+(g^+)a$]	−0.2	0.092	1.096
5(g^+)-B	[$g^-(g^+)a$]	−1.0	0.507	1.660
6(g^+)-B	[$a(g^+)a$]	0.0	0.000	1.000
7(g^+)-B	[$g^+(g^+)g^-$]	−2.3	1.157	3.181
8(g^+)-B	[$a(g^+)g^-$]	−1.0	0.495	1.641
9(g^+)-B	[$g^-(g^+)g^-$]	−1.4	0.706	2.027

Since D5 is associated with the rotation about the S−S bond, which usually assumes either +90° or −90°,[18] the potential energy hypersurface can be represented with two cross sections corresponding with D5 = +90° and D5 = −90° as seen in Figure 11. The optimized structures along with each of its own optimized thermodynamic functions are respectively given in the Supporting Information (Table S3a and Table S3b). The relative thermodynamic functions of the 2 × 9 = 18 optimized conformers are summarized in Table S3c and also shown graphically in Figure S5. It should be emphasized that the two levels shown in Figures 11 and S5 correspond to nine enantiomeric pairs. This is to be expected since clockwise or counterclockwise rotation represents chiral motion leading to axis chirality, also known as atropisomerism. In this context, axis chirality, that is the rotation to (+), i.e., P, such as g^+, or (−), i.e., M, such as g^-, direction may be related to S and R point chirality,[77,78] as defined in (13).

$$(+)\ \text{i.e. P} \rightarrow \text{S and } (-)\ \text{i.e. M} \rightarrow \text{R} \qquad (13)$$

The strength of the S−S linkages in the various conformations of diethyl disulfide have been measured by the following hydrogenation reaction 14:

$$\text{Et−S−S−Et} + \text{H}_2 \rightarrow 2\text{Et−SH} \qquad (14)$$

Figure 12 illustrates all the D4 = g^- conformers of diethyl disulfide. It should be noted that S−S bond length is somewhat longer in the crowded high-energy conformer and such a stretch of the S−S linkage appears to be necessary to reduce the steric repulsion between the two ethyl groups. The frequency and intensity values are listed in Table S4 of the Supporting Information in addition to the IR vibrational spectrum of the reference conformer [$a(g^+)a$] (Figure S2).

3.2.2. AIM Analysis of Electron Density Topology of Et−S−S−Et. Since the two sets of nine conformations [$x(g^+)y$] and [$x(g^-)y$] are enantiomeric, consequently only the nine conformers of the [$x(g^+)y$] family were subjected to AIMS analytics. The structures showing some of the parameters obtained by the AIM analysis are shown in Figure 13.

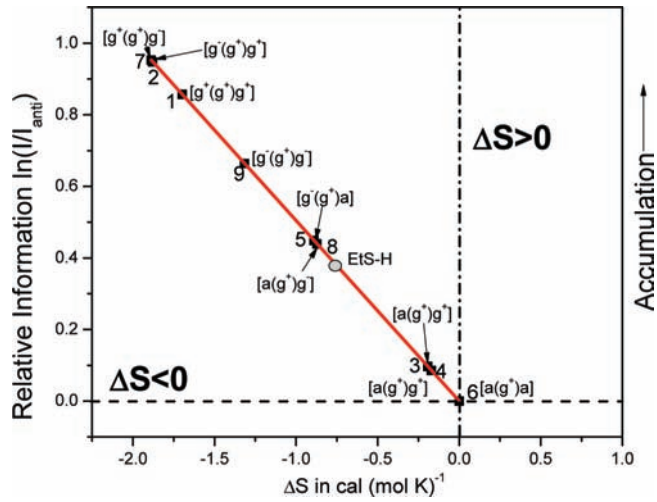

Figure 14. Clustering of Et−S−S−Et conformers according to the magnitude of their information accumulation.

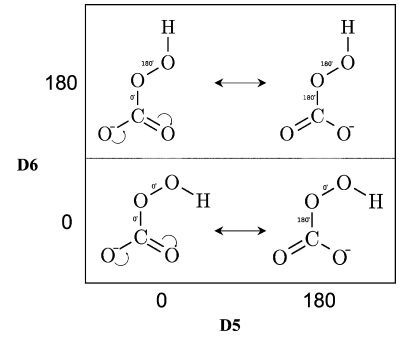

Figure 15. Two distinctly different conformers of HCO_4^-. The two columns are contributing resonance structures of carboxylic anion moiety results in two optimized structures even though D5 and D6 change between 0° and 180°.

3.2.3. Strength of the S−S Linkage. The stability of Et−S-S-Et may depend directly on the S−S bond length of disulfide, but it also depends on the existing nonbonded interactions established in the previous section. A hydrogenation reaction may yield an overall measure of stability:

$$\text{Et−S−S−Et} + \text{H}_2 \rightarrow 2\text{Et−SH} \qquad (15)$$

Since the product formed in a mildly exothermic reaction the greater a disulfide conformation stability the less exothermic is the above hydrogenation reaction as illustrated in Figure S6. Using the characteristics of H_2 (Table 3), we may arrive a set of ΔG and ΔS values of the reaction (Table 4). A graphical presentation of the results may be seen in Figure S7.

3.2.4. Structural Informational Content of Et−S−S−Et. Based on the relative entropy values given in Table S3c, the associated structural information content values are listed in Table 5.

The graphical presentation of the $\ln(I/I_{anti})$ values are shown in Figure 14.

3.3. Structural Analysis of Red−Ox Reagents. For the uncatalyzed reaction, H_2O_2/H_2O are the Red−Ox reagents and for the catalyzed reactions, those are the peroxybicarbonate/bicarbonate (HCO_4^-/ HCO_3^-). The geometrical parameters for HCO_4^-/ HCO_3^- are listed in the Supporting

Figure 16. Born−Haber summary of the thermodynamic reaction cycle involving the peroxybicarbonate and bicarbonate pair.

Information (Table S5) and graphically illustrated in Figure 15. The vibrational frequencies are given in Table S6. The computed thermodynamic functions are summarized in Tables S7 and S8 for HCO_4^- and HCO_3^-, respectively, in the Supporting Information. The geometrical parameters for the H_2O_2/H_2O system are given in Table S9 and the vibrational frequencies are listed in Table S10. Vibrational spectra of these two pairs of Red−Ox reagents are depicted in Figure S3. Thermodynamic functions for H_2O_2 and H_2O are presented in Table S11.

3.4. Energetics of the Red−Ox Reaction. The present two levels of theory applied (methods A and B) are expected to give different thermodynamic accuracy for the energetic change associated with the Red−Ox reaction. Nevertheless, in spite of the different, both of them are expected to be indicative of the exothermicity of the process. The details for the uncatalyzed reaction are given below:

$$2\text{Et}-\text{SH} + \text{H}_2\text{O}_2 + \text{H}_2 \rightarrow \text{Et}-\text{S}-\text{S}-\text{Et} + 2\text{H}_2\text{O} + \text{H}_2 \quad (16a)$$

$$\text{Et}-\text{S}-\text{S}-\text{Et} + 2\text{H}_2\text{O} + \text{H}_2 \rightarrow 2\text{Et}-\text{SH} + 2\text{H}_2\text{O} \quad (16b)$$

Overall:

$$\text{H}_2\text{O}_2 + \text{H}_2 \rightarrow 2\text{H}_2\text{O} \quad (16c)$$

Starting with the global minimum ($g^{\pm}$) of the reactant (Et−SH) and ending with any of the $2 \times 9 = 18$ minima, using the product (Et−S−S−Et), we may calculate the conformational dependent differences of the various thermodynamic functions (ΔF). The most important changes here are the ΔG and ΔS values of the Red−Ox process. This will give us three different ΔG and ΔS values according to the following equations.

$$\Delta F = \{F_{\text{Et-S-S-Et}}[x(g^+)y] + 2F_{\text{H}_2\text{O}} + F_{\text{H}_2}\} - \{2F_{\text{Et-SH}}[g^{\pm}] + F_{\text{H}_2\text{O}_2} + F_{\text{H}_2}\} \quad (17a)$$

$$\Delta F = \{2F_{\text{Et-SH}}[g^{\pm}] + 2\text{F}_{\text{H}_2\text{O}}\} - \{F_{\text{Et-S-S-Et}}[x(g^+)y] + 2F_{\text{H}_2\text{O}} + F_{\text{H}_2}\} \quad (17b)$$

$$\Delta F = \{2F_{\text{H}_2\text{O}}\} - \{\text{F}_{\text{H}_2\text{O}_2} + 2F_{\text{H}_2}\} \quad (17c)$$

Energetics for oxidation of Et−SH to Et−S−S−Et using the peroxybicarbonate/bicarbonate mechanism 17a where F is the energetics of all possible thermodynamic functions:

$$2\text{Et}-\text{SH} + \text{H}_2\text{O}_2 + \text{HCO}_3^- + \text{H}_2 \rightarrow 2\text{Et}-\text{SH} + \text{H}_2\text{O} + \text{HCO}_4^- + \text{H}_2 \quad (18a)$$

$$2\text{Et}-\text{SH} + \text{H}_2\text{O} + \text{HCO}_4^- + \text{H}_2 \rightarrow \text{Et}-\text{S}-\text{S}-\text{Et} + 2\text{H}_2\text{O} + \text{HCO}_3^- + \text{H}_2 \quad (18b)$$

$$\text{Et}-\text{S}-\text{S}-\text{Et} + 2\,\text{H}_2\text{O} + \text{HCO}_3^- + \text{H}_2 \rightarrow 2\text{Et}-\text{SH} + 2\text{H}_2\text{O} + \text{HCO}_3^- \quad (18c)$$

The sum total of the reaction is given in 18d:

$$\text{H}_2\text{O}_2 + \text{H}_2 \rightarrow 2\text{H}_2\text{O} \quad (18d)$$

The following equations specify the change in any thermodynamic function (F) that may be U, H, G, or S 17a:

$$\Delta F = \{2F_{\text{Et-SH}} + F_{\text{H}_2\text{O}} + F_{\text{HCO}_4^-} + F_{\text{H}_2}\} - \{2F_{\text{Et-SH}}[g^{\pm}] + F_{\text{HCO}_3^-} + F_{\text{H}_2\text{O}_2} + F_{\text{H}_2}\} \quad (19a)$$

$$\Delta F = \{F_{\text{Et-S-S-Et}}[x(g^+)y] + 2F_{\text{H}_2\text{O}} + F_{\text{HCO}_3^-} + F_{\text{H}_2}\} - \{2F_{\text{Et-SH}}[g^{\pm}] + F_{\text{HCO}_4^-} + F_{\text{H}_2\text{O}} + F_{\text{H}_2}\} \quad (19b)$$

$$\Delta F = \{2F_{\text{Et-SH}} + 2F_{\text{H}_2\text{O}} + F_{\text{HCO}_3^-}\} - \{\text{F}_{\text{Et-S-S-Et}}[x(g^+)y] + 2F_{\text{H}_2\text{O}} + F_{\text{HCO}_3^-} + F_{\text{H}_2}\} \quad (19c)$$

The overall change from initial to final state of the reaction 19d:

$$\Delta F = \{2F_{\text{H}_2\text{O}}\} - \{2F_{\text{H}_2\text{O}_2} + 2F_{\text{H}_2}\} \quad (19d)$$

All these reactions could be summarized in a Born−Haber thermodynamic cycle (Figure 16). The ΔG and ΔS differences are summarized in Table S5a. The corresponding energetic level diagram (Figure 17) illustrates the ΔG and ΔS values for the $[a(g^+)a]$ conformer of Et−S−S−Et.

3.5. Information Accumulation Associated with the Red−Ox Reaction. As it is apparent from eqs 16a and 18a, as well as Figures 16 and 17, that the direct oxidation of Et−SH to Et−S−S−Et by H_2O_2 is divided into two steps when bicarbonate is involved. In the first step, the bicarbonate is oxidized to peroxybicarbonate by H_2O_2 (i.e., $HCO_3^- \rightarrow HCO_4^-$). In the second step, ethyl mercaptan is oxidized to diethyl disulfide by HCO_4^- (i.e., 2Et−SH → Et−S−S−Et). It is noteworthy that both steps proceed with negative entropy change. The negative entropy change is related to an increased order information accumulation according to eq 11. The information accumulation is referring to structural meaning that Et−S−S−Et + $2H_2O$ is more ordered than two modes of EtSH + H_2O_2. Thus the elimination of the pathogenic peroxide from the system occurs with negative entropy change, therefore, implying Information Accumulation (Figure 18). In contrast to that, the hydrogenation of H_2O_2, as well as that of the oxidized form of the glutathione model (i.e., Et−S−S−Et), proceeds with positive entropy change thus with information depletion.

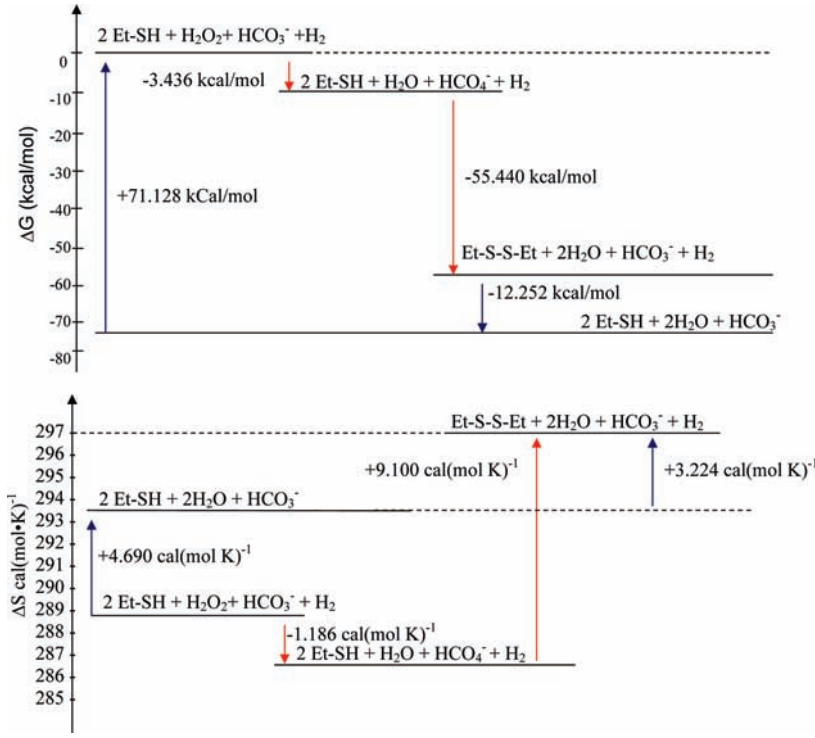

Figure 17. Changes in free energy (ΔG) and entropy (ΔS) values for the Red−Ox reaction of ethyl mercaptan and diethyl disulfide [$a(g^+)a$] computed using method A. The red and blue arrows correspond to the thermodynamic reaction cycle indicated in Figure 16.

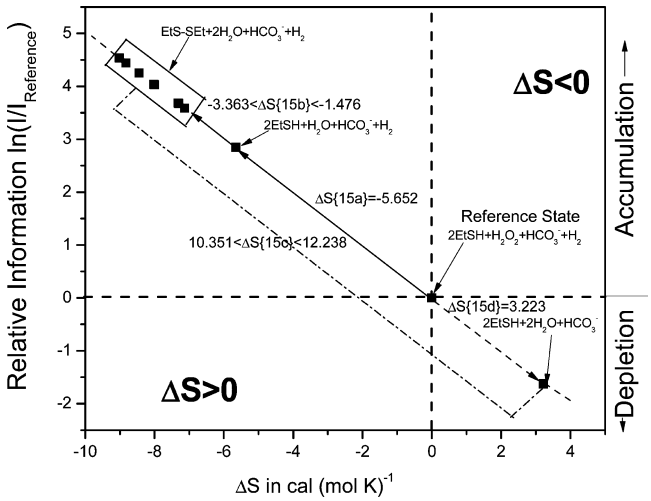

Figure 18. Information accumulation and information depletion associated with various Red−Ox reactions involving Et−SH and Et−S−S−Et using various reagents.

It has been previously noted that on going from a cancerous to a healthy cell, the entropy change is negative,[80,81] corresponding to information accumulation. Correspondingly, the dissociation of peptide parallel β-sheets that dominate the plaques in Alzheimer's Disease, governs negative entropy change.[3,17] Interestingly enough it has been shown in this paper that the elimination of the cancer-initiating as well as Alzheimer's Disease-initiating peroxide by the glutathione (GSH) model (Et−SH) also proceeds with negative entropy change and correspondingly with Information Accumulation.

3.6. Mechanistic Comparison. If we wishes to consider the oxidative reactions in a somewhat greater details we need comparing the two mechanisms presented in Figure 3. In both of these reactions there is an intermediate GSOH which we would need to model by EtSOH. Mechanism A in Figure 3A would be

$$\mathrm{Et{-}SH + HCO_4^- \rightarrow Et{-}SOH + HCO_3^-} \quad (20a)$$

$$\mathrm{Et{-}SOH + HS{-}Et \rightarrow Et{-}S{-}S{-}Et + H_2O} \quad (20b)$$

The analogous carbonate releasing mechanism B in Figure 3B, following the work of Regino and Richardson,[14] has already been presented in the form of eq 5a.

The computed thermodynamics functions are presented in Table S12 and the relative thermodynamic functions are given in Table 6. The first step of mechanism B is noticeable endothermic, due to the double negative charge of the carbonat ion. This endothermicity is expected to be reduced substantially upon solvatation.

TABLE 6: Relative Thermodynamics Functions (in kcal mol^{-1}) for Both Reaction Mechanisms Shown in Figure 3 and Specified in eqs *5a* and *20a*

reaction	ΔU	ΔH	ΔG
5a	120,3	120,3	120,0
5b	−17,9	−17,9	−16,5
20a	−38,6	−38,6	−39,0
20b	−17,9	−17,9	−16,5

4. Conclusions

The conformational space of ethyl mercaptan and diethyl disulfide was investigated. It has been found that the concept of axis chirality plays a significant role in determining the conformational PEHS topology in diethyl disulfide. The energetics of the following Red−Ox reactions:

$$Et-SH + HO-OH + HS-Et \rightarrow 2H_2O + Et-S-S-Et \quad (21a)$$

$$Et-SH + HO-OCOO^{(-)} + HS-Et \rightarrow H_2O + Et-S-S-Et + HCO_3^- \quad (21b)$$

mimicked the biologically important GSH Red-Ox reactions:

$$G-SH + H_2O_2 + HS-G \rightarrow 2H_2O + G-S-S-G \quad (22a)$$

$$G-SH + HCO_4^- + HS-G \rightarrow H_2O + G-S-S-G + HCO_3^- \quad (22b)$$

Through first principle molecular computations, the Red−Ox reaction of Et−SH → Et−S−S−Et was found to be exothermic at both levels of theory used [B3LYP/6-31G(d,p) and G3MP2B3]. It is hoped that such simple models may be useful in mimicking the complex bioactive molecules, such as GSH and GS−SG, since the thiol group (−SH) undergoes the greatest amount of chemical change during oxidation.

Acknowledgment. The authors would like to thank the Professor Suzanne Stevenson, Vice Dean of Arts & Science, for her support within the ROP Program at the University of Toronto. The continuous support of the Global Institute of Computational Molecular and Materials Science (www.giocomms.org) and the Drug Discovery Research Center (www.drugcent.com) are gratefully acknowledged.

GSH	glutathione, reduced
GSSG	glutathione, oxidized
Et-SH	ethyl mercaptan
Et−S−S−Et	diethyl disulfide
PEC	potential energy curve
PES	potential energy surface
PEHS	potential energy hypersurface

Supporting Information Available: Additional tables and figures. This material is available free of charge via the Internet at http://pubs.acs.org.

References and Notes

(1) Smith, T. J. *Renewal: The Anti-Aging revolution*; Rondale Press, Inc.: Emmaus, PA, 1998.
(2) Behrend, L.; Henderson, G.; Zwacka, R. M. *Biochem. Soc. Trans.* **2003**, *31*, 1441.
(3) Apel, K.; Hirt, H. *Annu. Rev. Plant Biol.* **2004**, *55*, 373.
(4) Bergamini, C. M.; Gambetti, S.; Dondi, A.; Cervellati, C. *Curr. Pharm. Des.* **2004**, *10*, 1611.
(5) Reddy, M. B.; Clark, L. I. *Nutr. Rev.* **2004**, *62*, 120.
(6) Shah, A. M.; Channon, K. M. *Heart* **2004**, *90*, 486.
(7) Willner, C. *Altern. Ther. Health. Med.* **2004**, *10*, 26.
(8) Wei, H. *Med. Hypotheses* **1992**, *39*, 267.
(9) Cerutti, P. A. *Lancet* **1994**, *344*, 862.
(10) Bohr, V. A.; Dianov, G. L. *Biochimie* **1999**, *81*, 155.
(11) Lieberman, S.; Bruning, N. *The Real Vitamin and Mineral Book*; Avery Publishing Group: New York, 1997.
(12) Strand, R. D. *Bionutrition*, 2nd ed.; Comprehensive Wellness Publishing: New York, 1998.
(13) Bayse, C. A. *J Phys. Chem. A* **2007**, *111*, 9070.
(14) Regino, C. A. S.; Richardson, D. E. *Inorg. Chim. Acta* **2007**, *360*, 3971.
(15) Dobson, C. M. *Trends Biochem. Sci.* **1999**, *24*, 329.
(16) Fändrich, M.; Forge, V.; Buder, K.; Kittler, M.; Dobson, C. M.; Diekmann, S. *Proc. Natl. Acad. Sci. U.S.A.* **2003**, *100*, 15463.
(17) Perczel, A.; Hudáky, P.; Pálfi, V. K. *J. Am. Chem. Soc.* **2007**, *129*, 14959.
(18) Eakin, C. M.; Berman, A. J.; Miranker, A. D. *Nat. Struct. Mol. Biol.* **2006**, *13*, 202.
(19) Dobson, C. M. *Nature* **2005**, *435*, 747.
(20) Lührs, T.; Ritter, C.; Adrian, M.; Riek-Loher, D.; Bohrmann, B.; Döbeli, H.; Schubert, D.; Riek, R. *Proc. Natl. Acad. Sci. U.S.A.* **2005**, *102*, 17342.
(21) Cohen, E.; Bieschke, J.; Perciavalle, R. M.; Kelly, J. W.; Dillin, A. *Science* **2006**, *313*, 1604.
(22) Barja, G. *Trends Neurosci.* **2004**, *27*, 595.
(23) Andersen, J. K. *Nat. Rev. Neurosci.* **2004**, 18.
(24) Owen, M. C.; Komaromi, I.; Murphy, R. F.; Lovas, S. *J. Mol. Struct. (THEOCHEM)* **2006**, *759*, 117.
(25) Owen, M.; Murphy, R. F.; Lovas, S. The conformational Preference of Ca-Centered Protein Radicals. In *Understanding Biology Using Peptides*. Proceedings of the Nineteenth American Peptide Symposium. Blondelle, S. E., Ed.; Springer: New York, 2006; pp 710−711.
(26) Schulz, J. B.; Lindenau, J.; Seyfried, J.; Dichgans, J. *Eur. J. Biochem.* **2000**, *267*, 4904.
(27) Vogelstein, B.; Kinzler, K. W. *Nat. Med.* **2004**, *10*, 789.
(28) Folkman, J.; Hahnfeldt, P.; Hlatky, L. *Nat. Rev. Mol. Cell Biol.* **2000**, *1*, 76.
(29) Soto, A. M.; Sonnenschein, C. *Bioessays* **2004**, *26*, 1097.
(30) Gibbs, W. *Sci. Am.* **2003**, *289*, 56.
(31) Jaffe, L. F. *Adv. Cancer Res.* **2003**, *90*, 209.
(32) Waris, G.; Ahsan, H. *J. Carcinogen.* **2006**, *5*, 14.
(33) López-Lázaro, M. *Cancer Lett.* **2007**, *252*, 1.
(34) Park, S.; You, X.; Imlay, J. A. *Proc. Natl. Acad. Sci. U.S.A.* **2005**, *102*, 9317.
(35) Hunt, C. R.; Sim, J. E.; Sullivan, S. J.; Featherstone, T.; Golden, W.; Kapp-Herr, C.; Rock, R. A.; Gomez, R. A.; Parsian, A. J.; Spitz, D. R. *Cancer Res.* **1998**, *58*, 3986.
(36) Jackson, A. L.; Loeb, L. A. *Mutat. Res.* **2000**, *447*, 187.
(37) Pericone, C. D.; Bae, D.; Shchepetov, M.; McCool, T.; Weiser, J. N. *J. Bacteriol.* **2002**, *184*, 4392.
(38) Henle, E. S.; Linn, S. *J. Biol. Chem.* **1997**, *272*, 19095.
(39) Imlay, J. A.; Linn, S. *Science* **1988**, *240*, 1302.
(40) Zanetti, M.; Katusic, Z. S.; O'Brien, T. *Am. J. Physiol. Heart Circ. Physiol* **2002**, *283*, H2620.
(41) Polytarchou, C.; Hatziapostolou, M.; Papadimitriou, E. *J. Biol. Chem.* **2005**, *280*, 40428.
(42) Brown, M. R.; Miller, F. J., Jr.; Li, W. G.; Ellingson, A. N.; Mozena, J. D.; Chatterjee, P.; Engelhardt, J. F.; Zwacka, R. M.; Oberley, L. W.; Fang, X.; Spector, A. A.; Weintraub, N. L. *Circ. Res.* **1999**, *85*, 524.
(43) Del Bello, B.; Paolicchi, A.; Comporti, M.; Pompella, A.; Maellaro, E. *FASEB J.* **1999**, *13*, 69.
(44) Qian, Y.; Luo, J.; Leonard, S. S.; Harris, G. K.; Millecchia, L.; Flynn, D. C.; Shi, X. *J. Biol. Chem.* **2003**, *278*, 16189.
(45) Arbiser, J. L.; Petros, J.; Klafter, R.; Govindajaran, B.; McLaughlin, E. R.; Brown, L. F.; Cohen, C.; Moses, M.; Kilroy, S.; Arnold, R. S.; Lambeth, D. *Proc. Natl. Acad. Sci. U.S.A.* **2002**, *99*, 715.
(46) Nelson, K. K.; Ranganathan, A. C.; Mansouri, J.; Rodriguez, A. M.; Providence, K. M.; Rutter, J. L.; Pumiglia, K.; Bennett, J. A.; Melendez, J. A. *Clin. Cancer Res.* **2003**, *9*, 424.
(47) Nishikawa, M.; Tamada, A.; Hyoudou, K.; Umeyama, Y.; Takahashi, Y.; Kobayashi, Y.; Kumai, H.; Ishida, E.; Staud, F.; Yabe, Y.; Takakura, Y.; Yamashita, F.; Hashida, M. *Clin. Exp. Metastasis* **2004**, *21*, 213.
(48) Chen, Q.; Espey, M. G.; Krishna, M. C.; Mitchell, J. B.; Corpe, C. P.; Buettner, G. R.; Shacter, E.; Levine, M. *Proc. Natl. Acad. Sci. U.S.A.* **2005**, *102*, 13604.
(49) Okamoto, M.; Kawai, K.; Reznikoff, C. A.; Oyasu, R. *Cancer Res.* **1996**, *56*, 4649.
(50) Suh, Y. A.; Arnold, R. S.; Lassegue, B.; Shi, J.; Xu, X.; Sorescu, D.; Chung, A. B.; Griendling, K. K.; Lambeth, J. D. *Nature* **1999**, *401*, 79.
(51) Arnold, R. S.; Shi, J.; Murad, E.; Whalen, A. M.; Sun, C. Q.; Polavarapu, R.; Parthasarathy, S.; Petros, J. A.; Lambeth, J. D. *Proc. Natl. Acad. Sci. U.S.A.* **2001**, *98*, 5550.
(52) Okamoto, M.; Reddy, J. K.; Oyasu, R. *Int. J. Cancer* **1997**, *70*, 716.
(53) Policastro, L.; Molinari, B.; Larcher, F.; Blanco, P.; Podhajcer, O. L.; Costa, C. S.; Rojas, P.; Durán, H. *Mol. Carcinog.* **2004**, *39*, 103.
(54) Yang, J. Q.; Buettner, G. R.; Domann, F. E.; Li, Q.; Engelhardt, J. F.; Weydert, C. D.; Oberley, L. W. *Mol. Carcinog.* **2002**, *33*, 206.
(55) Redegeld, F. A. M.; Koster, A. S.; Bennekon, W. P. Determination of Tissue Glutathione. In *Glutathione: Metabolism and Physiological Functions*; Viña, J., Ed.; CRC Press: Boston, 1990.

(56) Kosower, E. M. Chemical Properties of Glutathione. In *Glutathione: Metabolism and Function*; Arias, I. M., Jakoby, W. B., Eds.; Raven Press: New York, 1976.
(57) Hopkins, F. G. *J. Biol. Chem.* **1929**, *84*, 269.
(58) Glutathione. *The Merck Index*; Budavari, S., et al., Eds.; Merck Research Laboratories: New Jersey, 1996.
(59) Meister, A.; Anderson, M. E. *Annu. Rev. Biochem.* **1983**, *52*, 711.
(60) Taniguchi, M., Hirayama, K.; Yamaguchi, K.; Tateishi, N.; Suzuki M. Nutritional Aspects of Glutathione Metabolism and Function. In *Glutathione: Chemical, Biochemical, and Medical Aspects*; Dolphin, D., Poulson, R., Avramovic, O., Eds.; John Wiley & Sons: New York, 1989.
(61) Maetzke, A.; Jensen, S. J.; Csizmadia, I. G. *Chem. Phys. Lett.* **2007**, *448*, 46.
(62) Frisch, M. J., et al. *Gaussian 03 6.0* 2003, Gaussian, Inc.: Pittsburgh, PA.
(63) Sahai, M.; Szori, M.; Viskolcz, B.; Pai, E.; Csizmadia, I. G. J. *Phys. Chem. A* **2007**, *111*, 8384.
(64) Perczel, A.; Angyán, J. G.; Kajtar, M.; Viviani, W.; Rivail, J.; Marcoccia, J.; Csizmadia, I. G. *J. Am. Chem. Soc.* **1991**, *113*, 6256.
(65) Chass, G. A.; Marai, C. N. J.; Harrison, A. G.; Csizmadia, I. G. *J. Phys. Chem. A* **2002**, *106*, 9695 Beauchamp Dedication Issue.
(66) Tang, T.-H.; Deretey, E.; Knak Jensen, S. J.; Csizmadia, I. G. *Eur. Phys. J. D* **2006**, *37*, 217.
(67) Bader, R. F. W. *Acc. Chem. Res.* **1985**, *18*, 9.
(68) Bader, R. F. W. *Chem. Rev.* **1991**, *91*, 893.
(69) Csizmadia, I. G. *J. Mol. Struct. (THEOCHEM)* **2003**, *666*−*667*, 11.
(70) Viskolcz, B.; Fejer, S. N.; Szori, M.; Csizmadia, I. G. *Mol. Phys.* **2006**, *104*, 795.
(71) Viskolcz, B.; Fejer, S. N.; Csizmadia, I. G. *J. Phys Chem. A* **2006**, *110*, 3808.
(72) Fejer, S. N.; Csizmadia, I. G.; Viskolcz, B. *J. Phys. Chem. A* **2006**, *110*, 13325.
(73) Viskolcz, B.; Szori, M.; Izsak, R.; Fejer, S. N.; Csizmadia, I. G. *Int. J. Quantum Chem.* **2007**, *107*, 1826.
(74) Wolfe, S.; Tel, L. M.; Csizmadia, I. G. *J. Am. Chem. Soc.* **1973**, *95*, 4863.
(75) Csizmadia, I. G. General and Theoretical Aspects of the Thiol Group. In *The Chemistry of the Thiol Group*; Patai, S., Ed.; John Wiley and Sons: New York, 1974.
(76) Haworth, N. L.; Gready, J. E.; George, R. A.; Wouters, M. A. *Mol. Simul.* **2007**, *33*, 475.
(77) Lin, A. C.; Salpietro, S. J.; Deretey, E.; Csizmadia, I. G. *Can. J. Chem.* **2000**, *78*, 362.
(78) Csizmadia, I. G. *Basic Principles of Organic Chemistry*:; Quirk Press: Toronto, 1997; Vol. 2.
(79) Lide, D. R. *CRC Handbook of Chemistry and Physics, Internet Version 2005*; CRC Press: Boca Raton, FL, 2005; http://www.hbcpnetbase.com.
(80) Molnar, J. J.; Luo, L.; Ding, H.; Lv, X.; Spengler, G. *Diagnostic Pathol.* **2006**, *1*, 43.
(81) Molnar, J.; Thornton, B. S.; Molnar, A.; Gaál, D.; Luo, L.; Bergmann-Leitner, E. S. *Lett. Drug Des. Discovery* **2005**, *2*, 255.

JP809116N